The Protonation State of a Heme Propionate Controls Electron Transfer in Cytochrome *c* Oxidase†

Gisela Brändén,‡ Magnus Brändén,‡ Bryan Schmidt,§ Denise A. Mills,§ Shelagh Ferguson-Miller,§ and Peter Brzezinski*,‡

Department of Biochemistry and Biophysics, The Arrhenius Laboratories for Natural Sciences, Stockholm University, SE-106 91 Stockholm, Sweden, and Department of Biochemistry, Michigan State University, East Lansing, Michigan 48824

Received February 15, 2005; Revised Manuscript Received May 25, 2005

ABSTRACT: In cytochrome *c* oxidase (C*c*O), exergonic electron transfer reactions from cytochrome *c* to oxygen drive proton pumping across the membrane. Elucidation of the proton pumping mechanism requires identification of the molecular components involved in the proton transfer reactions and investigation of the coupling between internal electron and proton transfer reactions in C*c*O. While the proton-input trajectory in C*c*O is relatively well characterized, the components of the output pathway have not been identified in detail. In this study, we have investigated the pH dependence of electron transfer reactions that are linked to proton translocation in a structural variant of C*c*O in which Arg481, which interacts with the heme D-ring propionates in a proposed proton output pathway, was replaced with Lys (RK481 C*c*O). The results show that in RK481 C*c*O the midpoint potentials of hemes *a* and a_3 were lowered by ∼40 and ∼15 mV, respectively, which stabilizes the reduced state of Cu_A during reaction of the reduced C*c*O with O_2. In addition, while the pH dependence of the F → O rate in wild-type C*c*O is determined by the protonation state of two protonatable groups with pK_a values of 6.3 and 9.4, only the high-pK_a group influences this rate in RK481 C*c*O. The results indicate that the protonation state of the Arg481 heme a_3 D-ring propionate cluster having a pK_a of ∼6.3 modulates the rate of internal electron transfer and may act as an acceptor of pumped protons.

Redox-driven membrane-bound proton pumps use the free energy associated with reduction−oxidation (redox) reactions to translocate protons across a membrane, thereby maintaining a transmembrane electrochemical proton gradient that is used, for example, to produce ATP (for recent reviews, see refs *1*−*4*). So far, a complete molecular mechanism of proton pumping has not been uncovered in any redox-driven proton pump. In contrast to other proton transporters, the proton pumps do not use any carriers that would physically move the protons across the membrane. Instead, proton translocation (pumping) occurs through an energetic link between the exergonic electron transfer reactions from an electron donor to an acceptor, and the endergonic translocation of protons from the more negatively (*N*-) charged to the more positively (*P*-) charged side of the membrane (for recent reviews, see refs *2*−*5*). This type of energetic link may be provided, for example, by means of redox-induced changes in the pK_a of an intraprotein protonatable group(s). Proton translocation takes place if the changes in pK_a are temporally linked to changes in the proton connectivity to the two sides of the membrane (often called proton "gating"), e.g., through a rotation of the side chain of a protonatable amino acid residue, such that the group has a high pK_a when in contact with the proton-input (*N*-side) side and a low pK_a when in contact with the proton-output (*P*-side) side.

In the respiratory heme-copper oxidases, which constitute the last components of the respiratory chains of most aerobic organisms, the free energy for proton translocation is provided by electron transfer from an electron donor to oxygen, which is reduced to water. In cytochrome *c* oxidase (C*c*O)[1] from *Rhodobacter sphaeroides* (Figure 1), the electron donor is reduced cytochrome *c* (cyt *c*) and the primary electron acceptor is a copper center, Cu_A, located near the *P*-side surface of C*c*O. From Cu_A, electrons are transferred consecutively to a heme group (heme *a*) and to the binuclear center, which consists of a heme group (heme a_3) and a copper ion (Cu_B) and constitutes the enzyme's catalytic site. In its reduced state, the catalytic site binds the O_2 molecule, which is then reduced in a stepwise fashion by four electrons and four protons to water. Thus, the reaction

† This work was supported by grants from the Swedish Research Council (to P.B.), Human Frontier Science Program Grant RG0135 (to S.F.-M. and P.B.), and National Institutes of Health Grants GM 26916 and GM 20488 (to S.F.-M.).

* To whom correspondence should be addressed. Phone: (+46)-8 163280. Fax: (+46)-8 153679. E-mail: peterb@dbb.su.se.

‡ Stockholm University.

§ Michigan State University.

[1] Abbreviations: C*c*O, cytochrome *c* oxidase; Cu_A, copper A; Cu_B, copper B; binuclear center, heme a_3 and Cu_B; WT, wild type; R, cytochrome *c* oxidase with a fully reduced binuclear center; P_R, "peroxy" intermediate formed at the binuclear center upon reaction of the fully reduced cytochrome *c* oxidase with O_2; F, "oxo-ferryl" intermediate; O, fully oxidized enzyme; *N*-side, negative side of the membrane; *P*-side, positive side of the membrane; R481, arginine at position 481; RK481, replacement of R481 with lysine. Time constants are given as inverse rate constants. If not otherwise indicated, amino acid residues are numbered according to the *R. sphaeroides* cytochrome *c* oxidase sequence and the residues are found in subunit I.

10.1021/bi0502745 CCC: $30.25
Published on Web 07/14/2005

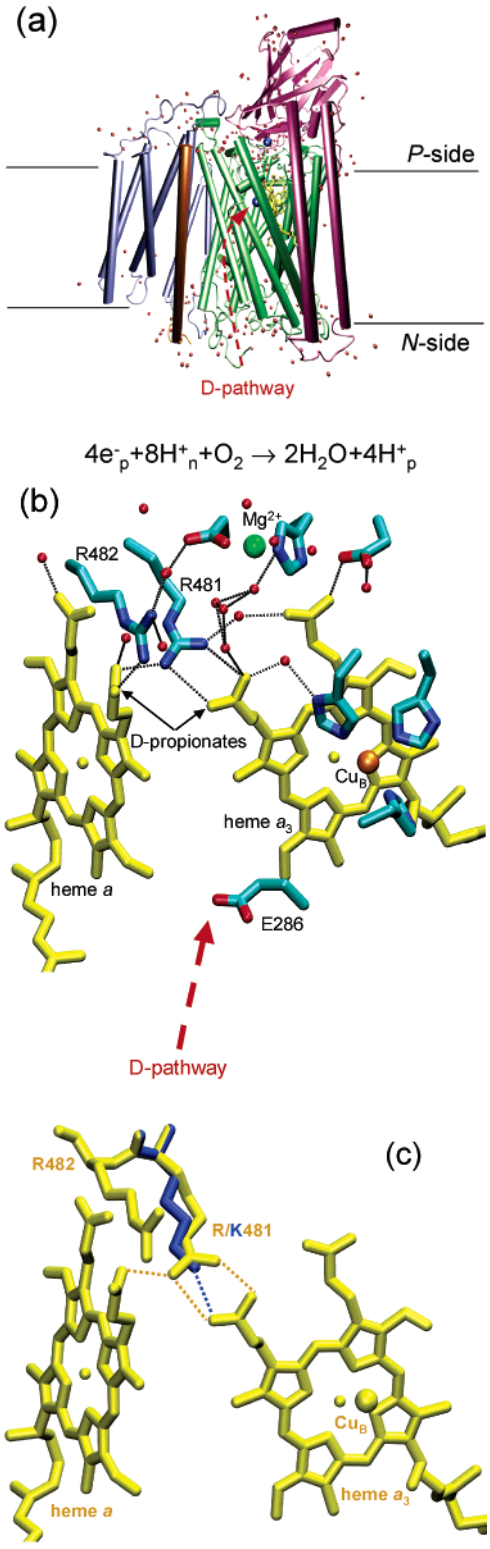

FIGURE 1: Structure of C*c*O (cytochrome aa_3) from *R. sphaeroides*. (a) Subunits I−IV are shown in different colors. Heme groups are colored yellow and copper ions blue. The approximate position of the proton transfer D-pathway is indicated. (b) Structure around the heme propionates and R481. (c) Modeled structure of the RK481 mutant overlaid on that of wild-type C*c*O. The C*c*O structure is that of the *R. sphaeroides* enzyme [Protein Data Bank entry 1m56 (*47*)]. This figure was prepared using Visual Molecular Dynamics (*48*).

catalyzed by C*c*O is

$$4\text{cyt } c_P^{2+} + O_2 + 4H_N^+ \rightarrow 4\text{cyt } c_P^{3+} + 2H_2O$$

where the subscripts *P* and *N* refer to the positive and negative sides of the membrane, respectively (the protons used in this reaction are called "substrate" protons). This reaction results in a charge separation corresponding to a movement of one positive charge from the *N*-side to the *P*-side per electron transferred to O_2. In addition, the reaction is linked to translocation of one proton per electron across the membrane, from the *N*-side to the *P*-side, resulting in a net stoichiometry of two translocated positive charges per electron transferred to O_2.

Two proton transfer pathways leading from the *N*-side surface toward the catalytic site are found in *R. sphaeroides* C*c*O; one is called the D-pathway (see Figure 1a,b), and one is called the K-pathway. The K-pathway is used for the uptake of one or two protons upon reduction of the catalytic site, while the D-pathway is used for the uptake of the remaining six or seven protons (*4*, *6*−*10*); i.e., the D-pathway is used for the uptake of both substrate and pumped protons. Consequently, at some position in the D-pathway, there must be a branching point from which protons are distributed either toward an acceptor of the pumped protons or toward the catalytic site. This branching point is presumably located at or near residue Glu286 in subunit I (E286) at the end of the D-pathway (Figure 1b) (*11*−*14*). One of the questions relating to the mechanism of proton pumping by C*c*O is the identity of the acceptor of pumped protons and how the proton transfer from E286 to this acceptor group is regulated. The results from a number of studies indicate that this acceptor is located in the area near the D-ring propionates of hemes *a* and a_3 (Figure 1b) (*13*, *15*−*19*; see also ref *20*). Electrostatic interactions with two Arg residues, Arg481 (R481) and Arg482 (R482) in subunit I, stabilize the anionic form of the propionates (*16*). The results from studies on site-directed mutants of *Escherichia coli* cytochrome bo_3 oxidase, in which these two Arg residues have been modified, suggested that destabilization of the anionic form of the heme a_3 D-ring propionate results in loss of proton pumping (*13*). In *R. sphaeroides* C*c*O, replacement of R481 with a Lys (see Figure 1c, i.e., the charge of the residue is not altered) did not result in a significant loss of activity or proton pumping in the absence of a membrane potential. The turnover activity under controlled conditions (i.e., with an electrochemical gradient across the membrane) of this mutant C*c*O, however, was much lower than that observed with wild-type C*c*O, resulting in a much higher respiratory control ratio (RCR)[2] for the mutant than for wild-type C*c*O. In addition, substitution of R481 and R482 with other amino acid residues resulted in alteration of the heme *a* midpoint potential (*21*−*23*).

As is evident from the results discussed above, the area around the D-ring heme propionates, R481, and R482 is presumably part of the pathway for translocated protons, and hence, transient structural and/or pK_a changes, during turnover of C*c*O, in this region might be part of the pumping machinery of C*c*O. In this study, we have investigated electron and proton transfer reactions during specific reaction transitions, in RK481 mutant C*c*O, that are temporally coupled to proton pumping (see Figure 2): the peroxy →

[2] The RCR is the ratio of the C*c*O turnover activities in the absence of a proton electrochemical gradient (with H^+ and K^+ ionophores) and in its presence (without H^+ and K^+ ionophores).

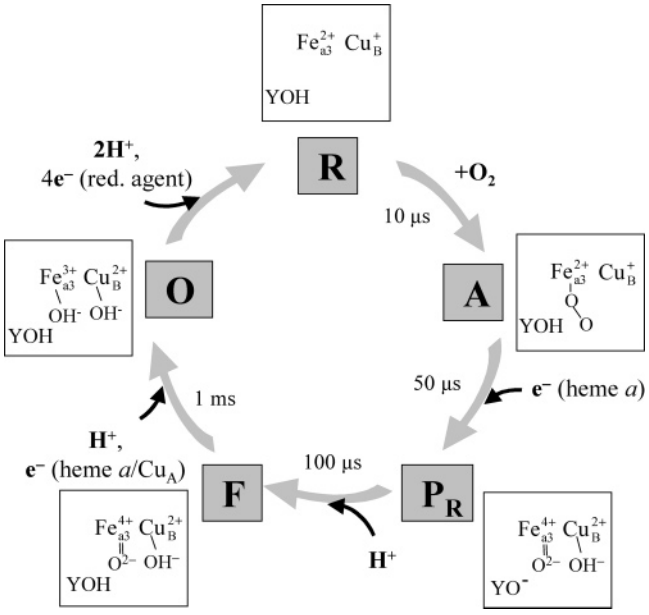

FIGURE 2: Reaction scheme showing the intermediate states during the reaction of the four-electron reduced C*c*O with O_2. The states of the catalytic site in each reaction intermediate are shown within the boxes. The oxidized C*c*O (state O) is fully reduced by four electrons (the two electrons that are transferred to heme *a* and Cu_A are not shown explicitly), associated with the uptake of approximately two protons. The following reaction is assumed to be initiated upon mixing the fully reduced (R) C*c*O with O_2 at ~1 mM. In the first step after O_2 binds to heme a_3, an electron is transferred from heme *a* to the catalytic site forming state P_R. Then a proton is taken up from the bulk solution, through E286, to the catalytic site forming state F. At the same time, the electron at Cu_A equilibrates with heme *a* (see the text). In the last reaction step, this electron is transferred to the catalytic site and a proton is taken up from the bulk solution to form the oxidized state (O). Y denotes Tyr288.

ferryl ($P_R \rightarrow F$) transition, which is associated only with proton transfer to the catalytic site, and the ferryl → oxidized ($F \rightarrow O$) transition, which is associated with electron and proton transfer to the catalytic site. The data indicate that the rate of the $F \rightarrow O$ transition is modulated by the protonation state of a group that is not part of the catalytic site. The RK481 mutation results in an alteration of the pK_a of this group, which is proposed to be the D-ring propionate of heme a_3.

MATERIALS AND METHODS

Enzyme Preparation. Histidine-tagged mutant and wild-type C*c*O were purified from *R. sphaeroides* as previously described (*24*), and the concentration was determined using UV−visible spectroscopy.

Potentiometric Titration of Heme a. Chemical redox titrations of heme *a* were performed essentially as described in ref *25*. The C*c*O was diluted to 1 μM in 100 mM phosphate buffer and 0.1% dodecyl β-D-maltoside (pH 7.0), and 5 mM KCN was added to stabilize the binuclear center in the oxidized state. The sample was then transferred to an anaerobic cuvette in which the electrodes were immersed, and the air was exchanged for N_2 gas. The redox mediators Ferrocene, PMS (phenazine methosulfate), and Quinhydrone were added, each at a concentration of 20 μM, reducing heme *a* completely. Small aliquots of potassium ferricyanide were added to slowly oxidize heme *a*, and for each reduction potential value, the A(605 nm) − A(620 nm) absorbance difference was determined. The sample was then gradually re-reduced using potassium ferrocyanide and sodium dithionite to check that the original starting absorbance for the fully reduced heme *a* had not changed.

Potentiometric Titration of Heme a_3. Redox phototitrations of heme a_3 were performed using cytochrome *c* (from horse heart) as the redox indicator and riboflavin as the photoreductant, as described in ref *26*. The C*c*O was diluted to 3 μM in 100 mM HEPES buffer and 0.1% DDM (pH 7.4), and 2 mM EDTA, 30 μM riboflavin, 15 μM cytochrome *c*, and 6 μM ferricyanide were added. The sample was placed in an anaerobic cuvette, and the air was exchanged for N_2 gas, keeping the sample in the dark at all times to prevent reduction of the light-sensitive riboflavin. Electrons were introduced into the system by short light pulses, gradually reducing riboflavin, cytochrome *c*, and C*c*O, and after each illumination, an absorbance spectrum between 400 and 700 nm was recorded after the system reached equilibrium. Finally, sodium dithionite was added to check that the sample was fully reduced. The midpoint potential of heme a_3 was determined using cytochrome *c* as a reduction potential standard (fixed at 260 mV).

*Preparation of the Fully Reduced CO-Bound C*c*O.* The C*c*O buffer was exchanged on a PD-10 desalting column (Amersham Biosciences) for 100 mM KCl, 0.1 mM HEPES-KOH, and 0.1% dodecyl β-D-maltoside (pH 7.5), with a final enzyme concentration of 10 μM. Then 0.2 μM PMS was added, and the sample was transferred to an anaerobic cuvette, which was repeatedly evacuated on a vacuum line and flushed with N_2. The C*c*O was reduced with 5 mM ascorbate, and the N_2 was exchanged for CO.

Flow-Flash Kinetic Measurements. The C*c*O−CO complex was rapidly mixed at a 1:5 ratio with an O_2-saturated buffer solution in a stopped-flow apparatus. The pH after mixing was set by the buffer solution, which contained 100 mM MES, HEPES-KOH, Tris-HCl, CHES, or CAPS, depending on the pH, and 0.1% dodecyl β-D-maltoside. Approximately 200 ms after mixing, the CO ligand was dissociated using a short laser flash at 532 nm (Quantel, Brilliant B), and the reaction was monitored by recording the absorbance changes at a number of single wavelengths: 445, 580, 605, and 830 nm. This custom-built stopped-flow/flash-photolysis apparatus (Applied Photophysics, Leatherhead, Surrey, U.K.) is described in more detail in ref *27*. The data were analyzed using PRO-K (Applied Photophysics).

Proton Uptake Measurements. The C*c*O was prepared as described above, with the exception that buffer was excluded and the pH dye phenol red (40 μM) was added before reduction with ascorbate. After CO had bound to C*c*O, the pH was adjusted to 7.6. The kinetics of proton uptake was followed at 560 nm, as described in ref *8*.

RESULTS

In this study, we have investigated specific electron and proton transfer reactions, during oxidation of the reduced C*c*O by O_2, that are associated with proton pumping and net proton uptake from the bulk solution.

Since the interpretation of the results requires knowledge of any differences between the thermodynamic properties

of the mutant and those of wild-type C*c*O, we first determined the midpoint potentials of hemes *a* and a_3 in RK481 C*c*O. The midpoint potential of heme *a* in C*c*O in which CN^- is bound to heme a_3 was ~40 mV lower than that of wild-type C*c*O. The midpoint potential of heme a_3 was ~15 mV lower than in wild-type C*c*O (not shown).

Panels a and b of Figure 3 show absorbance changes at 445 and 580 nm, respectively, associated with oxidation of the reduced wild-type and RK481 mutant C*c*O after flash photolysis of CO in the presence of O_2. The temporally unresolved absorbance change at time zero is associated with the dissociation of CO from reduced heme a_3. At 445 and 580 nm, the decrease in absorbance observed in the time range from 0 to ~100 μs is associated with binding of O_2 to reduced heme a_3 (R → A transition, $\tau \cong 10$ μs), and thereafter by oxidation of heme *a* and formation of the peroxy state (A → P_R transition, $\tau \cong 50$ μs) (cf. Figure 2).

With wild-type C*c*O, the subsequent increase in absorbance at 580 nm (Figure 3b) is associated with formation of the ferryl intermediate (P_R → F transition, $\tau \cong 100$ μs). This transition is also associated with a fractional (~50%) electron transfer from Cu_A to heme *a*. The oxidation of Cu_A is seen as a kinetic phase with a time constant of ~100 μs at 830 nm (Figure 3c, an increase in absorbance at 830 nm corresponds to oxidation of Cu_A), preceded by a lag corresponding to the R → P_R transitions (see the time range from 0 to ~100 μs). During the P_R → F transition, proton uptake from the bulk solution also occurs on the same time scale, as seen from the increase in the absorbance of the pH-sensitive dye phenol red at 560 nm (Figure 3d).

All absorbance changes on time scales up to P_R formation were the same with the RK481 as with the wild-type C*c*Os. The increase in absorbance at 580 nm in the time range of 50−200 μs with RK481 mutant C*c*O shows that the F state was formed with the same time constant (100 μs) as with wild-type C*c*O. In both the wild-type and mutant C*c*Os, formation of F was accompanied by proton uptake (Figure 3d). As seen in Figure 3c, in the RK481 mutant C*c*O at 830 nm, no kinetic phase with a time constant of 100 μs was observed; i.e., the P_R → F transition was not coupled to oxidation of Cu_A, which is also consistent with the smaller absorbance increase at 580 nm (the reduction of heme *a* contributes with an increase in absorbance at 580 nm in wild-type C*c*O). This lack of electron transfer from Cu_A to heme *a* during the P_R → F transition in the mutant C*c*O is also evident from a comparison of the absorbance changes at 445 nm (Figure 3a) in the time range from ~0 to 0.5 ms (P_R → F transition). At 445 nm, formation of P_R was associated with a decrease in absorbance in both the wild-type and mutant C*c*Os. Because in the wild-type C*c*O the heme *a* re-reduction during the P_R → F transition results in an increase in absorbance, the net decrease in absorbance is greater in the RK481 mutant than in wild-type C*c*O. The smaller reduction extent of heme *a* in the RK481 mutant C*c*O is consistent with the lower midpoint potential of heme *a* (see above and accompanying paper by Mills et al.).

The slowest transition, F → O ($\tau \cong 1.6$ ms), is seen as a decrease in absorbance at 445 and 580 nm. On the same time scale, there is an increase in absorbance at 830 nm associated with oxidation of reduced Cu_A (Figure 3c). This increase was larger with the RK481 mutant than with wild-type C*c*O because in the former Cu_A was oxidized in the entire enzyme population (cf. the absence of Cu_A oxidation on the time scale of the previous, P_R → F, transition). The transition was also associated with proton uptake from the bulk solution (Figure 3d). The F → O reaction displayed the same time constant with RK481 and wild-type C*c*O at pH 7.5.

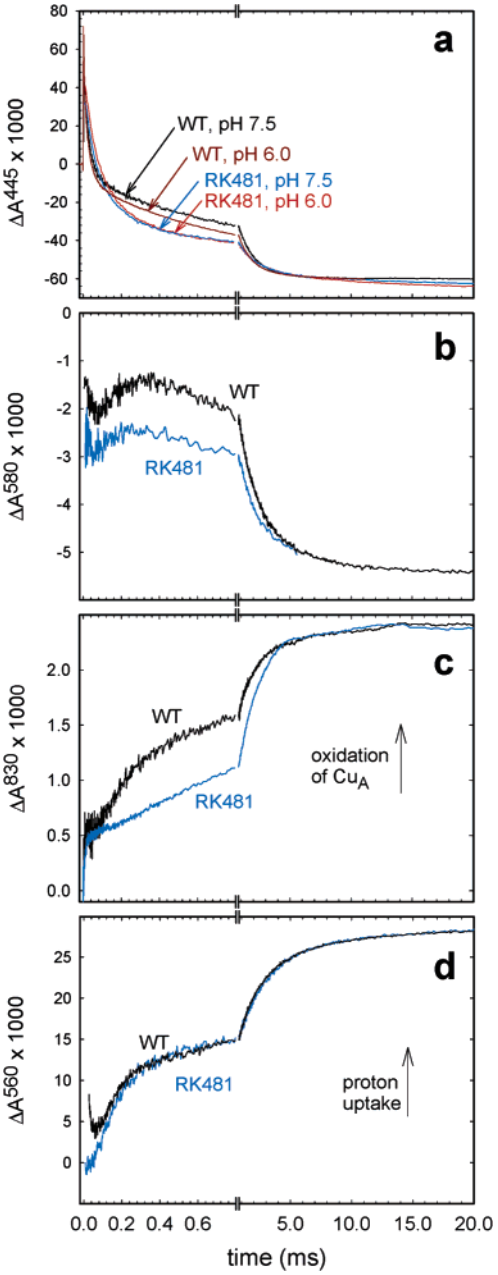

FIGURE 3: Absorbance changes associated with the reaction of the fully reduced wild-type (WT) and RK481 mutant C*c*O with O_2. The absorbance changes at 445 (a) and 580 nm (b) are mainly associated with the redox reaction of the heme groups and ligand binding to heme a_3. At 830 nm (c), the absorbance changes are mainly associated with oxidation of Cu_A (increase in absorbance). (d) Absorbance changes at 560 nm (of the pH dye) are associated with proton uptake during oxidation of the fully reduced C*c*O. Experimental conditions: ~2 μM reacting enzyme (all traces have been normalized to 1 μM reacting enzyme), 0.1 M HEPES-KOH (pH 7.5), or 0.1 M MES (pH 6.0) [except for panel d where the buffer was replaced with 0.1 M KCl and the pH dye phenol red at 40 μM (pH 7.6)], 0.1% dodecyl β-D-maltoside, and 1 mM O_2 at 22 °C.

Figure 4a shows the pH dependence of the P_R → F rate in wild-type (*28*, *29*) and RK481 mutant C*c*O. Results from

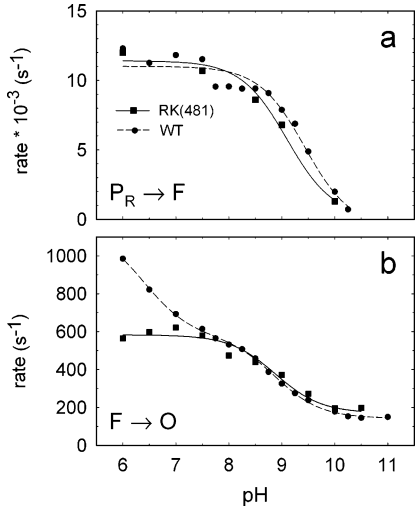

FIGURE 4: pH dependence of the $P_R \rightarrow F$ (a) and $F \rightarrow O$ (b) rates during reaction of the fully reduced wild-type (WT) and RK481 mutant C*c*O with O_2. The transition rates were obtained from traces at 445 and 580 nm (see Figure 3). The solid (RK481) and dashed (wild-type) lines are fits with eqs A1 (in panel a) and A10 (in panel b) from the Appendix, using the following parameters: (a) wild-type, $k_H^0 = 1.1 \times 10^4$ s^{-1} and p$K_E = 9.4$; RK481, $k_H^0 = 1.1 \times 10^4$ s^{-1} and p$K_E = 9.1$; and (b) wild-type, $K_3^0 = 0.1$, $K_1 = 1$, $\delta E \cong 30$ mV, p$K_E = 8.9$, p$K_X = 6.3$, and $k_0 = 120$ s^{-1}; RK481, $K_3^0 = 0.26$, $K_1 = 0.22$, $\delta E \cong 30$ mV, p$K_E = 8.9$, p$K_X < 5$, and $k_0 = 120$ s^{-1}. Experimental conditions: ~2 μM reacting enzyme, 0.1 M MES (pH 6.0 or 6.5), HEPES-KOH (pH 7.0 or 7.5), Tris-HCl (pH 8.0 or 8.5), CHES (pH 9.0 or 9.5), or CAPS (pH 10.0 or 10.5), 0.1% dodecyl β-D-maltoside, and 1 mM O_2 at 22 °C.

earlier experiments indicate that the pK_a of 9.4, observed in the pH dependence of the rate of this reaction, is an apparent pK_a of E286 in the proton transfer D-pathway (*28*, *29*) (see Discussion). The pK_a observed in the pH dependence of the $P_R \rightarrow F$ rate in RK481 mutant C*c*O was ~9.1.

As shown previously, the $F \rightarrow O$ rate, measured with wild-type C*c*O, decreases with an increase in pH (Figure 4b), and the trace can be fitted with a titration curve displaying two pK_a values of 6.3 ± 0.3 and 8.9 ± 0.1 (*29*). As shown in Figure 4b, with the RK481 mutant C*c*O, the rate of the $F \rightarrow O$ transition followed that of wild-type C*c*O in the pH range of 8−10.5, where the observed pK_a was ~8.9, i.e., the same as the high pK_a observed with wild-type C*c*O. Below pH 8 (in the pH range of 6−8), the rate did not depend on pH; i.e., the lower pK_a titration point observed with wild-type C*c*O was not seen with RK481 C*c*O (see also the traces obtained with RK481 and wild-type C*c*O at 445 nm shown in Figure 3a).

DISCUSSION

The focus of this study is the elucidation of the proton-exit pathway of C*c*O. We have investigated the effect of a mutation of R481, interacting (electrostatically) with the D-ring heme *a* and a_3 propionates, on the pH dependencies of specific reaction steps that are linked to proton pumping.

Effect of Structural Alterations in RK481 Mutant CcO on Its Functional Properties. In wild-type C*c*O, the two amino groups of R481 form ionic bonds with the two oxygen atoms of the heme a_3 D-propionate. In addition, one of the amino groups interacts electrostatically with one of the heme *a* D-propionates (Figure 1b). According to molecular dynamics simulations, replacement of R481 with a Lys, having only one amino group, results in loss of the interaction with the heme *a* D-propionate leaving only an interaction with the heme a_3 D-propionate (see the accompanying paper by Seibold et al.) (Figure 1c). When considering only the electrostatics of the protein, qualitatively, this scenario is consistent with the decrease in the heme *a* midpoint potential of ~40 mV that we observe because in the RK481 mutant C*c*O the positive charge distribution at R481 is removed from the heme *a* D-propionate. Even though the change in the charge density around the heme a_3 propionate is expected to result in a stronger interaction between the Lys and the heme a_3 D-ring propionate, the midpoint potential of heme a_3 is decreased by ~15 mV, which is presumably an effect of the structural alterations themselves.

It has been observed that the formyl group of heme *a*, which is part of the π-electron system, interacts strongly with the protein environment (*30*). Mutation of Arg54 (*Paracoccus denitrificans* C*c*O numbering), which interacts with the heme *a* formyl group in *P. denitrificans* C*c*O, resulted in a large spectral shift of heme *a* and a large decrease in its midpoint potential (*31*−*33*). Alterations in the heme *a* spectral properties were also observed in the corresponding mutant of *R. sphaeroides* C*c*O (*34*). The much smaller effect on the properties of heme *a* in the RK481 mutant C*c*O is consistent with the more conservative mutation and the fact that the propionates are not part of the π-electron system.

Proton Transfer during the $P_R \rightarrow F$ Transition. Formation of the P_R state involves electron transfer from heme *a* to the catalytic site ($\tau \cong 50$ μs; see Figure 2). The following $P_R \rightarrow F$ transition at the catalytic site, with a time constant of ~100 μs, is associated with proton transfer from solution to the catalytic site (Figure 3d). The proton is presumably transferred initially from E286 (or water molecules around E286) to the catalytic site, followed by rapid reprotonation of this group from bulk solution (*35*). Therefore, the observed pK_a in the pH dependence of the $P_R \rightarrow F$ rate reflects that of E286, and the maximum rate of the transition at low pH is the rate of proton transfer from E286 to the catalytic site (see the Appendix) (*28*, *29*). An investigation of the pH dependence of the $P_R \rightarrow F$ transition rate showed that it could be fitted with a Henderson−Hasselbach titration curve with a single pK_a of 9.4 and a maximum rate of 1.1×10^4 s^{-1} (*28*).

The results in Figure 4a show that with RK481 mutant C*c*O the pH dependence of the $P_R \rightarrow F$ rate was very similar (p$K_a \cong 9.1$) to that of wild-type C*c*O. In addition, a proton was taken up from the bulk solution with a rate that was the same as that of the $P_R \rightarrow F$ transition (see Figure 3d). These results indicate that the proton transfer rate through the D-pathway is not slowed in the RK481 mutant C*c*O and that the pK_a of E(I-286) is approximately the same as in wild-type C*c*O.

Electron Transfer from Cu_A to Heme a during the $P_R \rightarrow F$ Transition. As discussed above, in wild-type C*c*O two events take place on the time scale of the $P_R \rightarrow F$ transition ($\tau \cong$ 100 μs): proton transfer from solution to the catalytic site and fractional electron transfer from Cu_A to heme *a*. The proton is initially transferred from E286 to the catalytic site, followed by rapid reprotonation of E286 from the bulk solution. Results from earlier studies showed that the electron transfer from Cu_A to heme *a* cannot take place if E286 remains in the unprotonated state (*8*, *36*). In other words, if

E286 is not reprotonated, the midpoint potential of heme *a*, relative to that of Cu_A, is lowered, presumably due to the excess negative charge at the E286 site.

The data in Figure 3 show that in RK481 mutant C*c*O the electron is not transferred from Cu_A to heme *a* on the time scale of the $P_R \rightarrow F$ transition. As the E286 residue is reprotonated during formation of F in the mutant C*c*O (see above), the lack of electron transfer from Cu_A to heme *a* is explained in terms of the lower intrinsic midpoint potential of heme *a*. In wild-type C*c*O, the midpoint potentials of Cu_A and heme *a* during the $P_R \rightarrow F$ transition are approximately equal (~50% of Cu_A becomes oxidized; see Figure 3c). In RK481 mutant C*c*O, the heme *a* midpoint potential was ~40 mV lower than in wild-type C*c*O. Assuming that the midpoint potential of Cu_A is not altered in RK481 mutant C*c*O, the data are consistent with the absence of Cu_A to heme *a* electron transfer with a time constant of 100 μs ($P_R \rightarrow F$ transition).

The F → O Rate. The $F \rightarrow O$ transition involves both electron (the fourth electron) and proton transfer from the bulk solution, through the D-pathway, to the catalytic site. As both the electron and the proton are required for formation of the O state, the transition rate is dependent on the fraction of the fourth electron residing at the catalytic site and the proton transfer rate to the catalytic site (*14*, *37*). The fraction of electrons at the catalytic site is determined by the equilibrium of the electron among Cu_A, heme *a*, and the catalytic site. One question that arises is the effect of lowering the midpoint potentials of hemes *a* and a_3 by ~40 and ~15 mV, respectively, on the fraction of electrons at the catalytic site and thus on the observed $F \rightarrow O$ rate. This question is addressed in the Appendix, and the calculations show that at pH 7.5 the $F \rightarrow O$ rate is not expected to change significantly when these midpoint potentials are lowered.

The proton transfer reaction during the $F \rightarrow O$ transition is assumed to take place via the same mechanism that is used during the $P_R \rightarrow F$ transition (see above); i.e., the rate is proportional to the fraction of protonated E286 (see above). Thus, the pH dependence of the $F \rightarrow O$ rate reflects pH-dependent changes in both the electron equilibrium and the proton transfer reaction. As seen in Figure 4, the pH dependence of this rate with wild-type C*c*O cannot be fitted with a single Henderson−Hasselbach titration curve and the protonation state of two protonatable sites with apparent pK_a values of 6.3 and 8.9 must be assumed to control the rate (*29*). The higher pK_a (8.9) is similar to that determined from the pH dependence of the $P_R \rightarrow F$ rate (9.4). Studies of mutant C*c*Os, in which residues in the D-pathway were altered, showed an equal change in pK_a for the $P_R \rightarrow F$ transition rate and the $F \rightarrow O$ transition rate (ref *38* and unpublished results of A. Namslauer et al.). Therefore, we assign the high pK_a in the pH titration of the $F \rightarrow O$ rate to E286. The lower pK_a (6.3), not observed in the pH dependence of the $P_R \rightarrow F$ transition rate, is attributed to the electron transfer component of the $F \rightarrow O$ rate, i.e., the fraction of electrons at the catalytic site. The pH dependence of the electron equilibrium is presumably determined by a modulation of the midpoint potential of at least one of the redox sites (heme a_3; see below), e.g., through electrostatic interactions between the redox site and a protonatable group in its vicinity.

Assuming interactions between a single protonatable site and a redox site, qualitatively the midpoint potential of the redox site should increase with a decrease in pH because at low pH the positive charge of the protonatable group would be stabilized, which would stabilize the reduced state of the redox site. As seen in the Appendix (Figure 5a), an increase in the midpoint potential of heme *a*, as would be observed upon decreasing the pH, results in a decrease in the $F \rightarrow O$ rate, which is not consistent with the data in Figure 4b. Therefore, we assume that the protonatable group involved here interacts with heme a_3. Since the low-pH titration (pK_a ≅ 6.3) was not observed in the RK481 mutant C*c*O, the D-ring heme a_3 propionate is a likely candidate for the protonation site in wild-type C*c*O. In the mutant C*c*O, there is a larger positive charge density around the heme a_3 D-ring propionate due to the position of K481 as compared to R481 (see Figure 1c). This change in the charge density is expected to destabilize the protonated state of the propionate in the RK481 C*c*O, that is, to shift the pH range at which the propionate titrates to a lower value than in wild-type C*c*O. This scenario would explain the absence of the low-pH (pK_a ≅ 6.3) titration in the RK481 mutant C*c*O in the measured pH range.

Links between changes in the protonation state of a heme propionate and the midpoint potential have been observed in other systems (*39*, *40*). In C*c*O from bovine heart, the yields of states P and F were found to depend on the protonation state of a group with a pK_a similar to that observed for the low-pH titration in this work (*41*, *42*). Additionally, a link between changes in the redox state of specific groups and the protonation state of C*c*O have been noted and discussed (*43*, *44*).

Proton Pumping. As discussed above, results from both experimental and theoretical studies indicate that the region around the heme D-ring propionates and residues R481 and R482 is on the pathway of protons that are pumped by C*c*O. One question that arises in this context is why the RK481 mutant C*c*O pumps protons with approximately the same stoichiometry as wild-type C*c*O. It should be noted that proton pumping measurements are carried out in the absence of a membrane potential where the resistance for the transfer of pumped protons is much smaller than in the presence of a potential (*23*). Under these conditions, an alteration of the pK_a of a proton donor or acceptor in the pathway of pumped protons might not have an effect on the pumping stoichiometry. Consequently, the effect of the mutation might be manifested only in the presence of an electrochemical proton gradient. This notion is supported by the observation that the turnover activity of the mutant C*c*O is approximately the same as that of wild-type C*c*O in the absence of a membrane potential, while in the presence of a potential, the rate is much slower with the mutant than with wild-type C*c*O [RCR values of ~35 and ~10 in the RK481 and wild-type C*c*Os, respectively (*21*, *22*)].

The pK_a of ~6.3 of the heme a_3 D-propionate proton acceptor might seem too low to be physiologically relevant. However, it should be noted that the pK_a is obtained from a kinetic measurement, and therefore, it might reflect an apparent pK_a of a process that involves other reactions that are linked to protonation and/or deprotonation of the group (*45*). The measured pK_a would then reflect the true intrinsic pK_a of the group together with the free energy change of

the reaction that is linked to the proton transfer. In addition, the local structure around the propionate may change during the proton transfer to provide proton accessibility to the input side first and then to the proton output side (cf. proton "gating"), which would result in modulation of the pK_a during the proton pumping event (see the detailed discussion in ref *45*). Moreover, if the group is connected to the outside, positive side of the membrane through a "proton well" [i.e., a pathway that conducts protons but not any other ions (*46*)], the apparent pH near the group might be shifted to a lower value than that in the outside bulk solution, which would require the involvement of a low-pK_a group in the proton pumping process.

In conclusion, the results from this study indicate that the protonation state of the heme a_3 D-ring propionate determines the rate of electron transfer to the catalytic site in C*c*O. These data provide insights into the functional design of the proton pumping machinery of C*c*O and the thermodynamic parameters of the components that are involved.

ACKNOWLEDGMENT

We thank Pia Ädelroth, Robert Cukier, and Steve Seibold for critically reading the manuscript and for valuable discussions and Ida Holmgren for technical assistance.

APPENDIX

The $P_R \rightarrow F$ Rate

The $P_R \rightarrow F$ transition involves a proton transfer from solution to the catalytic site through the D-pathway. The overall rate of F formation, k_{PF}(pH), is modeled to be determined by the fraction of protonated E286, α_{EH}(pH), times the rate of proton transfer from E286 to the catalytic site, k_H^0.

$$k_{PF}(\mathrm{pH}) = k_H^0 \times \alpha_{EH}(\mathrm{pH}) \quad \text{(A1a)}$$

$$\alpha_{EH}(\mathrm{pH}) = \frac{1}{1 + 10^{\mathrm{pH}-\mathrm{p}K_E}} \quad \text{(A1b)}$$

where pK_E is the pK_a of E286 (9.4; see the text) and k_H^0 was found to be 1.1×10^4 s^{-1} (see the text). Because the rate of the $P_R \rightarrow F$ transition and pK_E in the pH dependence are essentially the same with mutant and wild-type C*c*O, the proton transfer through the D-pathway is presumably not affected by the RK481 mutation.

The $F \rightarrow O$ Transition

The $F \rightarrow O$ Rate as a Function of the Midpoint Potential of Heme a. As discussed in the main text, the $F \rightarrow O$ rate is determined by the fraction of electrons at the catalytic site and the rate of proton transfer from E286 to the catalytic site when E286 is in its protonated state, α_{EH,F^-}. Neither the proton transfer rate through the D-pathway nor the pK_a of E286 is affected by the RK481 mutation. To determine the fraction of the reduced catalytic site, we consider the electron equilibrium in the F state between redox sites Cu_A and heme *a* and the catalytic site (a negative sign indicates a reduced redox site; we use the notion F^- to denote the fraction of electrons at the catalytic site). At pH 7.6, i.e., when E286 is protonated, the following model is used:

$$Cu_A{}^- aF \overset{K_1}{\longleftrightarrow} Cu_A a^- F \overset{K_3}{\longleftrightarrow} Cu_A aF^- \xrightarrow{k_H^0} Cu_A a\mathbf{O} \quad \text{(A2)}$$

where k_H^0 is the rate of proton transfer from E286 to the catalytic site. The equilibrium constants K_1 and K_2 are

$$K_1 = 10^{(E_a - E_{CuA})/60} \quad \text{(A3a)}$$

$$K_3 = 10^{(E_F - E_a)/60} \quad \text{(A3b)}$$

where E_a, E_{Cu_A}, and E_F are the midpoint potentials (in millivolts) of heme *a*, Cu_A, and the catalytic site, respectively. We tentatively call E_F the apparent midpoint potential of the catalytic site in the F state. The value is not a real midpoint potential as the accepting group is a transiently formed ferryl intermediate.

The fraction of reduced catalytic site is

$$\alpha_{EH,F^-} = [Cu_A aF^-] = \frac{10^{(E_F - E_{CuA})/60}}{1 + 10^{(E_a - E_{CuA})/60} + 10^{(E_F - E_{CuA})/60}} \quad \text{(A4)}$$

The observed $F \rightarrow O$ rate, k_{FO}, is

$$k_{FO} = \alpha_{EH,F^-} \times k_H^0 \quad \text{(A5)}$$

In Figure 5 is plotted k_{FO} as a function of the difference in the midpoint potentials of heme *a* and Cu_A with the proton transfer rate, k_H^0, fixed at 10^4 s^{-1}. In wild-type C*c*O, $E_F - E_{Cu_A}$ is set at -55 mV because this value gives an experimentally observed $F \rightarrow O$ rate ($\sim$570 s^{-1}, WT in Figure 5) for $E_a - E_{Cu_A} \cong 0$, where the potential difference has been determined experimentally (see the main text). Note that the $F \rightarrow O$ rate is relatively insensitive to changes in the heme *a* midpoint potential for negative $E_a - E_{Cu_A}$ values. In the RK481 mutant C*c*O, the midpoint potential of heme a_3 is $\sim$15 mV lower than in wild-type C*c*O; therefore, $E_F - E_{Cu_A}$ is set at -70 mV. Because the heme *a* midpoint potential is $\sim$40 mV lower than in wild-type C*c*O, $E_a - E_{Cu_A} \cong -40$ mV. The obtained $F \rightarrow O$ rate is $\sim$530 s^{-1} (RK in Figure 5), i.e., very similar to that obtained with wild-type C*c*O.

pH Dependence of the $F \rightarrow O$ Rate. Here, we use a more general model (see eq A4) that includes the unprotonated form of E286. For simplicity, we assume that the pK_a of E286, pK_E, is independent of the reduction state of C*c*O. All states in the top and bottom parts of the scheme are with unprotonated (E^-) and protonated (EH) E286, respectively.

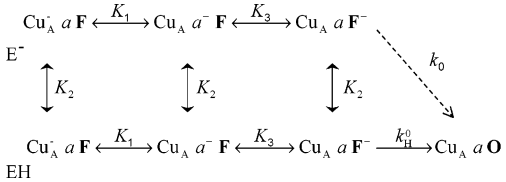

(A6)

The equilibrium constant K_1 is the same as that given above in eq 3a. K_2 is determined by the pK_a of E286, pK_E:

$$K_2(\mathrm{pH}) = 10^{\mathrm{p}K_E - \mathrm{pH}} \quad \text{(A7)}$$

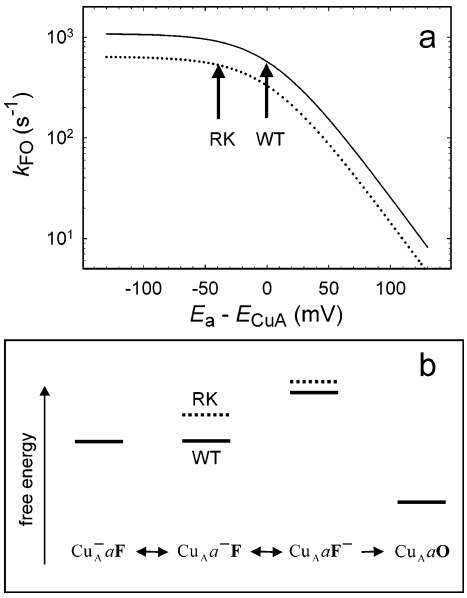

FIGURE 5: (a) Simulation of the F → O formation rate (k_{FO}) as a function of the difference in the heme *a* and Cu_A midpoint potentials, calculated using eq A5. The difference in the midpoint potentials of the electron-accepting group at the catalytic site (E_F) and that of Cu_A was fixed at −55 and −70 mV for the wild-type and RK481 mutant C*c*Os, respectively (see the text). (b) Energy diagram showing schematically the relative free energy changes associated with the transitions between the states shown in the bottom part of the diagram. The midpoint potentials of hemes *a* and a_3 are decreased by ∼40 and ∼15 mV, respectively, in the RK481 (RK) mutant C*c*O.

For K_3, we assume that the catalytic site interacts electrostatically with a protonatable group, X, such that

$$E_F = E_F^0 + \delta E \times \gamma(\mathrm{pH}) \quad \text{(A8a)}$$

$$\gamma(\mathrm{pH}) = \frac{1}{1 + 10^{\mathrm{pH}-\mathrm{p}K_X}} \quad \text{(A8b)}$$

where E_F^0 is the midpoint potential of the catalytic site with unprotonated X, δE is the interaction energy (in millivolts) between X and the catalytic site, and pK_X is the pK_a of X. Thus

$$K_3(\mathrm{pH}) = 10^{\{[E_F{}^0+\delta E\times\gamma(\mathrm{pH})]-E_a\}/60} = K_3^0 \times 10^{[\delta E\times\gamma(\mathrm{pH})]/60} \quad \text{(A9a)}$$

where

$$K_3^0 = 10^{(E_F{}^0-E_a)/60} \quad \text{(A9b)}$$

i.e., the equilibrium constant between the catalytic site and heme *a* with unprotonated X. The fraction of C*c*O with electrons at the catalytic site and with protonated E286 is

$$\alpha_{EH,F^-} = \frac{K_1K_2K_3}{1 + K_1 + K_2 + K_1K_3 + K_1K_2 + K_1K_2K_3} \quad \text{(A10)}$$

and the observed rate, k_{FO}, is

$$k_{FO} = \alpha_{EH,F^-} \times k_H^0 + k_0 \quad \text{(A11)}$$

where k_0 is the proton transfer rate though the D-pathway with unprotonated E286 (i.e., at pH >11).

REFERENCES

1. Mills, D. A., Florens, L., Hiser, C., Qian, J., and Ferguson-Miller, S. (2000) Where is 'outside' in cytochrome *c* oxidase and how and when do protons get there? *Biochim. Biophys. Acta 1458*, 180−187.
2. Wikström, M. (2004) Cytochrome *c* oxidase: 25 years of the elusive proton pump, *Biochim. Biophys. Acta 1655*, 241−247.
3. Brzezinski, P. (2004) Redox-driven membrane-bound proton pumps, *Trends Biochem. Sci. 29*, 380−387.
4. Gennis, R. B. (2004) Coupled proton and electron transfer reactions in cytochrome oxidase, *Front. Biosci. 9*, 581−591.
5. Ferguson-Miller, S., and Babcock, G. T. (1996) Heme/copper terminal oxidases, *Chem. Rev. 96*, 2889−2907.
6. Ruitenberg, M., Kannt, A., Bamberg, E., Ludwig, B., Michel, H., and Fendler, K. (2000) Single-electron reduction of the oxidized state is coupled to proton uptake via the K pathway in *Paracoccus denitrificans* cytochrome *c* oxidase, *Proc. Natl. Acad. Sci. U.S.A. 97*, 4632−4636.
7. Ädelroth, P., Gennis, R. B., and Brzezinski, P. (1998) Role of the pathway through K(I-362) in proton transfer in cytochrome *c* oxidase from *R. sphaeroides*, *Biochemistry 37*, 2470−2476.
8. Ädelroth, P., Svensson Ek, M., Mitchell, D. M., Gennis, R. B., and Brzezinski, P. (1997) Glutamate 286 in cytochrome aa_3 from *Rhodobacter sphaeroides* is involved in proton uptake during the reaction of the fully-reduced enzyme with dioxygen, *Biochemistry 36*, 13824−13829.
9. Konstantinov, A. A., Siletsky, S., Mitchell, D., Kaulen, A., and Gennis, R. B. (1997) The roles of the two proton input channels in cytochrome *c* oxidase from *Rhodobacter sphaeroides* probed by the effects of site-directed mutations on time-resolved electrogenic intraprotein proton transfer, *Proc. Natl. Acad. Sci. U.S.A. 94*, 9085−9090.
10. Wikström, M., Jasaitis, A., Backgren, C., Puustinen, A., and Verkhovsky, M. I. (2000) The role of the D- and K-pathways of proton transfer in the function of the haem-copper oxidases, *Biochim. Biophys. Acta 1459*, 514−520.
11. Hofacker, I., and Schulten, K. (1998) Oxygen and proton pathways in cytochrome *c* oxidase, *Proteins 30*, 100−107.
12. Iwata, S., Ostermeier, C., Ludwig, B., and Michel, H. (1995) Structure at 2.8 Å resolution of cytochrome *c* oxidase from *Paracoccus denitrificans*, *Nature 376*, 660−669.
13. Puustinen, A., and Wikström, M. (1999) Proton exit from the heme-copper oxidase of *Escherichia coli*, *Proc. Natl. Acad. Sci. U.S.A. 96*, 35−37.
14. Ädelroth, P., Karpefors, M., Gilderson, G., Tomson, F. L., Gennis, R. B., and Brzezinski, P. (2000) Proton transfer from glutamate 286 determines the transition rates between oxygen intermediates in cytochrome *c* oxidase, *Biochim. Biophys. Acta 1459*, 533−539.
15. Michel, H. (1999) Cytochrome *c* oxidase: Catalytic cycle and mechanisms of proton pumping-A discussion, *Biochemistry 38*, 15129−15140.
16. Kannt, A., Roy, C., Lancaster, D., and Michel, H. (1998) The coupling of electron transfer and proton translocation: Electrostatic calculations on *Paracoccus denitrificans* cytochrome *c* oxidase, *Biophys. J. 74*, 708−721.
17. Popovic, D. M., and Stuchebrukhov, A. A. (2004) Electrostatic study of the proton pumping mechanism in bovine heart cytochrome *c* oxidase, *J. Am. Chem. Soc. 126*, 1858−1871.
18. Behr, J., Hellwig, P., Mäntele, W., and Michel, H. (1998) Redox Dependent Changes at the Heme Propionates in Cytochrome *c* Oxidase from *Paracoccus denitrificans*: Direct Evidence from FTIR Difference Spectroscopy in Combination with Heme Propionate ^{13}C Labeling, *Biochemistry 37*, 7400−7406.
19. Wikström, M., Verkhovsky, M. I., and Hummer, G. (2003) Water-gated mechanism of proton translocation by cytochrome *c* oxidase, *Biochim. Biophys. Acta 1604*, 61−65.
20. Siegbahn, P. E. M., Blomberg, M. R. A., and Blomberg, M. L. (2003) Theoretical study of the energetics of proton pumping and oxygen reduction in cytochrome oxidase, *J. Phys. Chem. B 107*, 10946−10955.
21. Mills, D. A., Schmidt, B., Hiser, C., Westley, E., and Ferguson-Miller, S. (2002) Membrane Potential-controlled Inhibition of Cytochrome *c* Oxidase by Zinc, *J. Biol. Chem. 277*, 14894−14901.

22. Mills, D. A., and Ferguson-Miller, S. (2002) Influence of structure, pH and membrane potential on proton movement in cytochrome oxidase, *Biochim. Biophys. Acta 1555*, 96−100.
23. Qian, J., Mills, D. A., Geren, L., Wang, K., Hoganson, C. W., Schmidt, B., Hiser, C., Babcock, G. T., Durham, B., Millett, F., and Ferguson-Miller, S. (2004) Role of the conserved arginine pair in proton and electron transfer in cytochrome *c* oxidase, *Biochemistry 43*, 5748−5756.
24. Mitchell, D. M., and Gennis, R. B. (1995) Rapid purification of wildtype and mutant cytochrome *c* oxidase from *Rhodobacter sphaeroides* by Ni^{2+}-NTA affinity chromatography, *FEBS Lett. 368*, 148−150.
25. Dutton, P. L. (1978) Redox potentiometry: Determination of midpoint potentials of oxidation−reduction components of biological electron-transfer systems, *Methods Enzymol. 54*, 411−435.
26. Zickermann, V., Verkhovsky, M., Morgan, J., Wikström, M., Anemüller, S., Bill, E., Steffens, G. C., and Ludwig, B. (1995) Perturbation of the Cu_A site in cytochrome *c* oxidase of *Paracoccus denitrificans* by replacement of Met227 with isoleucine, *Eur. J. Biochem. 234*, 686−693.
27. Brändén, M., Sigurdson, H., Namslauer, A., Gennis, R. B., Ädelroth, P., and Brzezinski, P. (2001) On the role of the K-proton transfer pathway in cytochrome *c* oxidase, *Proc. Natl. Acad. Sci. U.S.A. 98*, 5013−5018.
28. Namslauer, A., Aagaard, A., Katsonouri, A., and Brzezinski, P. (2003) Intramolecular proton-transfer reactions in a membrane-bound proton pump: The effect of pH on the peroxy to ferryl transition in cytochrome *c* oxidase, *Biochemsitry 42*, 1488−1498.
29. Namslauer, A., and Brzezinski, P. (2004) Structural elements involved in electron-coupled proton transfer in cytochrome *c* oxidase, *FEBS Lett. 567*, 103−110.
30. Babcock, G. T., and Callahan, P. M. (1983) Redox-linked hydrogen bond strength changes in cytochrome *a*: Implications for a cytochrome oxidase proton pump, *Biochemistry 22*, 2314−2319.
31. Kannt, A., Pfitzner, U., Ruitenberg, M., Hellwig, P., Ludwig, B., Mäntele, W., Fendler, K., and Michel, H. (1999) Mutation of Arg-54 strongly influences heme composition and rate and directionality of electron transfer in *Paracoccus denitrificans* cytochrome *c* oxidase, *J. Biol. Chem. 274*, 37974−37981.
32. Jasaitis, A., Backgren, C., Morgan, J. E., Puustinen, A., Verkhovsky, M. I., and Wikström, M. (2001) Electron and proton transfer in the arginine-54-methionine mutant of cytochrome *c* oxidase from *Paracoccus denitrificans*, *Biochemistry 40*, 5269−5274.
33. Riistama, S., Verkhovsky, M. I., Laakkonen, L., Wikström, M., and Puustinen, A. (2000) Interaction between the formyl group of heme *a* and arginine 54 in cytochrome aa_3 from *Paracoccus denitrificans*, *Biochim. Biophys. Acta 1456*, 1−4.
34. Lee, H. M., Das, T. K., Rousseau, D. L., Mills, D., Ferguson-Miller, S., and Gennis, R. B. (2000) Mutations in the putative H-channel in the cytochrome *c* oxidase from *Rhodobacter sphaeroides* show that this channel is not important for proton conduction but reveal modulation of the properties of heme *a*, *Biochemistry 39*, 2989−2996.
35. Smirnova, I. A., Ädelroth, P., Gennis, R. B., and Brzezinski, P. (1999) Aspartate-132 in cytochrome *c* oxidase from *Rhodobacter sphaeroides* is involved in a two-step proton transfer during oxoferryl formation, *Biochemistry 38*, 6826−6833.
36. Karpefors, M., Ädelroth, P., Zhen, Y., Ferguson-Miller, S., and Brzezinski, P. (1998) Proton uptake controls electron transfer in cytochrome *c* oxidase, *Proc. Natl. Acad. Sci. U.S.A. 95*, 13606−13611.
37. Ädelroth, P., Ek, M., and Brzezinski, P. (1998) Factors Determining Electron-Transfer Rates in Cytochrome*c* Oxidase: Investigation of the Oxygen Reaction in the *R. sphaeroid*es and Bovine Enzymes, *Biochim. Biophys. Acta 1367*, 107−117.
38. Gilderson, G., Aagaard, A., and Brzezinski, P. (2002) Relocation of an internal proton donor in cytochrome *c* oxidase results in an altered pK_a and a non-integer pumping stoichiometry, *Biophys. Chem. 98*, 105−114.
39. Leitch, F. A., Moore, G. R., and Pettigrew, G. W. (1984) Structural basis for the variation of pH-dependent redox potentials of *Pseudomonas* cytochromes *c*-551, *Biochemistry 23*, 1831−1838.
40. Louro, R. O., Bento, I., Matias, P. M., Catarino, T., Baptista, A. M., Soares, C. M., Carrondo, M. A., Turner, D. L., and Xavier, A. V. (2001) Conformational component in the coupled transfer of multiple electrons and protons in a monomeric tetraheme cytochrome, *J. Biol. Chem. 276*, 44044−44051.
41. Fabian, M., Skultety, L., Jancura, D., and Palmer, G. (2004) Implications of ligand binding studies for the catalytic mechanism of cytochrome *c* oxidase, *Biochim. Biophys. Acta 1655*, 298−305.
42. Vygodina, T., and Konstantinov, A. (1989) Effect of pH on the spectrum of cytochrome *c* oxidase hydrogen peroxide complex, *Biochim. Biophys. Acta 973*, 390−398.
43. Capitanio, N., Vygodina, T. V., Capitanio, G., Konstantinov, A. A., Nicholls, P., and Papa, S. (1997) Redox-linked protolytic reactions in soluble cytochrome-c oxidase from beef-heart mitochondria: Redox Bohr effects, *Biochim. Biophys. Acta 1318*, 255−265.
44. Mitchell, R., and Rich, P. R. (1994) Proton uptake by cytochrome *c* oxidase on reduction and on ligand binding, *Biochim. Biophys. Acta 1186*, 19−26.
45. Brzezinski, P., and Larsson, G. (2003) Redox-driven proton pumping by heme-copper oxidases, *Biochim. Biophys. Acta 1605*, 1−13.
46. Mitchell, P. (1968) *Chemiosmotic Coupling and Energy Transduction*, Glynn Research Ltd., Bodmin, U.K.
47. Svensson-Ek, M., Abramson, J., Larsson, G., Törnroth, S., Brzezinski, P., and Iwata, S. (2002) The X-ray Crystal Structures of Wild-Type and EQ(I-286) Mutant Cytochrome *c* Oxidases from *Rhodobacter sphaeroides*, *J. Mol. Biol. 321*, 329−339.
48. Humphrey, W., Dalke, A., and Schulten, K. (1996) VMD: Visual Molecular Dynamics, *J. Mol. Graphics 14*, 33.

BI0502745